Journal of Molecular Liquids 336 (2021) 116263

Contents lists available at ScienceDirect

Journal of Molecular Liquids

journal homepage: www.elsevier.com/locate/molliq

Simulations of electroosmotic flow in charged nanopores using Dissipative Particle Dynamics with Ewald summation

Igor M. Telles, Rogério K. Bombardelli, Alexandre P. dos Santos, Yan Levin

Instituto de Física, Universidade Federal do Rio Grande do Sul, Caixa Postal 15051, CEP 91501-970 Porto Alegre, RS, Brazil

ARTICLE INFO

Article history:
Received 6 January 2021
Revised 14 April 2021
Accepted 19 April 2021
Available online 27 April 2021

Keywords:
Eletroosmosis
Electrolyte
Nanopore
Ewald
DPD

ABSTRACT

We present a Dissipative Particle Dynamics simulation method that allows us to study electroosmotic flows inside cylindrical nanopores with uniform surface charge. To properly treat the long-range electrostatic interactions between all the charges, we use two different approaches. In the first approach, the uniform surface charge is represented using surface point sites. The Coulomb interaction is then treated using 3d Ewald summation with an appropriate correction for the pseudo 1d geometry. In the second approach, the surface charge is treated implicitly. It produces an *external potential* in which all other particles move. In the case of an infinite cylinder, the electric field produced by a uniform surface charge vanishes. However, the rest of the system is no longer charge neutral. This requires an additional correction to the Ewald summation method. Since the second method does not use the explicit surface charges, it is about 40% more efficient – while producing identical electroosmotic flow and ionic charge distribution inside the pore.

1. Introduction

The long-range nature of the Coulomb potential prevents us from using simple periodic boundary conditions when performing computer simulations of charged systems. Instead, one needs to periodically replicate the system in order to achieve the proper thermodynamic limit. Unfortunately, the electrostatic energy of an infinitely replicated system is very difficult to calculate because of the slow convergence of the conditional sum over the replicas. To resolve this issue, the Coulomb potential is usually split into short and long-range contributions. The short-range summation is then performed in the real space, while the long-range summation can be efficiently performed in the reciprocal Fourier space [1–3]. The 3d Ewald summation is the most widely used method [4–11] to perform calculations of electrostatic energy of an infinitely replicated system, often with some alternative method to accelerate the calculation of the long-range interaction [12–18]. Such approaches have been widely used to perform simulations of bulk electrolyte and colloidal systems [19–23] and of ionic liquids [24–30]. When the full 3d replication symmetry is broken – such as when a system is confined between planar surfaces, or inside an infinite cylindrical pipe – a correction must be introduced to the 3d Ewald method, if one wants to use it within the restricted geometry [4,31–33]. The correction in the case of neutral charged systems was obtained for slab in Refs. [28,33–36], (2D aspect ratio) and for linear periodic geometry in Refs. [37–42], (1D aspect ratio). For non-neutral charged systems with slab geometry the correction was obtained in references [4,43–45].

In the present paper we will use Dissipative Particle Dynamics (DPD) simulations to study electroosmotic flows inside cylindrical nanopores with uniform surface charge. To properly treat the long-range electrostatic interactions between all the charges, we will use two different approaches. In the first approach the uniform surface charge will be represented using surface point sites. The Coulomb interaction will then be treated using 3d Ewald summation with an appropriate correction for the pseudo 1d geometry. In the second approach, the surface charge will be treated implicitly, resulting in an effective external potential that acts on all the ions inside the pore. The advantage of such approach is that one does not need to explicitly consider the surface charges. This lowers the total number of charged particles inside the system, significantly speeding up the calculations. In the case of an infinitely long pore, application of the Gauss law shows that the electric field produced by a uniform surface charge is zero. However, the absence of explicit surface charges results in a system that is no longer charge neutral. This requires an additional modification of the Ewald method to account for the pseudo 1d periodicity of a non-neutral nanopore system. We will show how the appropriate correction can be easily obtained from our previous results on Ewald systems with the restricted geometry [33]. The

E-mail address: alexandre.pereira@ufrgs.br (A.P. dos Santos)

https://doi.org/10.1016/j.molliq.2021.116263
0167-7322/

second approach is found to be about 40% more efficient, while remaining equally accurate.

The paper is organized as follows. In the Section 2, the DPD simulation method for infinitely long charged nanopores is introduced. In the Section 3, the modified Ewald method used to calculate the electrostatic forces in a periodic pseudo 1d geometry is presented. In Section 4, we introduce a simple mean-field theory to compare with the simulations. Finally, in Sections 5 and 6 we present the results and conclusions of the work, respectively.

2. Dissipative particle dynamics simulations

The DPD simulations are performed using a well established algorithm described in Refs. [46–48]. Conservative, friction, and random forces act together in a coarse grained way satisfying the fluctuation-dissipation theorem. Ions and surface charges are also considered as DPD particles, but with a charge at the center. The Coulomb interaction between all the charges in a periodically replicated system is included using the approach presented in the following section. The DPD parameters considered in our simulations are the same as in the previous works [46]. The mass of all particles is considered the same, m. Together with m and $\beta = 1/k_BT$, the Bjerrum length $\lambda_B = e^2/\epsilon k_BT$ is the natural unit used in the integration of dynamical equations of motion. In the present work we set $\lambda_B = 7.2$Å, value for water at room temperature. In order to consider the hard core nature of ionic particles, a regular Lennard-Jones force is included with the minimal distance $\sigma_{lj} = 0.6\lambda_B$ and strength $\varepsilon = 0.5k_BT$. All particles are confined inside a cylinder of radius R and length L_z, oriented along the z axis. Periodic boundary conditions are used in z direction. For Coulomb interaction between the particles, the cylinder is infinitely replicated along the z-axis, with periodicity L_z, so that each charged particle inside the simulation cell also interacts with an infinite number of its periodic replicas and with the replicas of all the other particles. No-slip boundary conditions are implemented at $r = R$, the radial distance measured from the central axis, using bounce-back method [49]. For ions we consider the effective distance of closest approach to the surface, $r = R - d$, where $d = \sigma_{lj}/2$. The number of solvent particles N_s is defined in terms of the bulk concentration ρ_s. In the present work we will set $\rho_s\lambda_B^3 = 3$. The number of counterions N_c of charge $-e$ inside the system also defines the surface charge density $\sigma > 0$ of the cylinder surface, $eN_c = \sigma 2\pi RL_z$. Besides the counterions, $N_\pm$ ions of charge e and $-e$ can be added in the form of a dissociated salt. When surface point charges are considered, they are distributed uniformly over the cylinder surface at $r = R + d$, see Fig. 1. The electroosmotic flow is induced with a constant electric field applied along the z direction, $\beta\lambda_B eE_z = 1$. In Fig. 2 we show a typical fluid concentration profile, together with the temperature profile. For all the cases studied, these curves are very similar.

3. Electrostatic calculations

We start by considering a general 3d Ewald summation method. Consider N charged particles q_j located at positions $\mathbf{r}_j = (x_j, y_j, z_j)$ in a rectangular box of sides L_p, L_p and L_z. This simulation box is replicated in all directions. The electrostatic potential at the position $\mathbf{r} = (x, y, z)$ can be written as [33]

$$\phi(\mathbf{r}) = \sum_{\mathbf{k}}^{\infty}\sum_{j=1}^{N}\frac{4\pi q_j}{\epsilon V|\mathbf{k}|^2}exp\left[-\frac{|\mathbf{k}|^2}{4\kappa_e^2} + i\mathbf{k}\cdot(\mathbf{r}-\mathbf{r}_j)\right] + \sum_{j=1}^{N} q_j\frac{erfc(\kappa_e|\mathbf{r}-\mathbf{r}_j|)}{\epsilon|\mathbf{r}-\mathbf{r}_j|}, \quad (1)$$

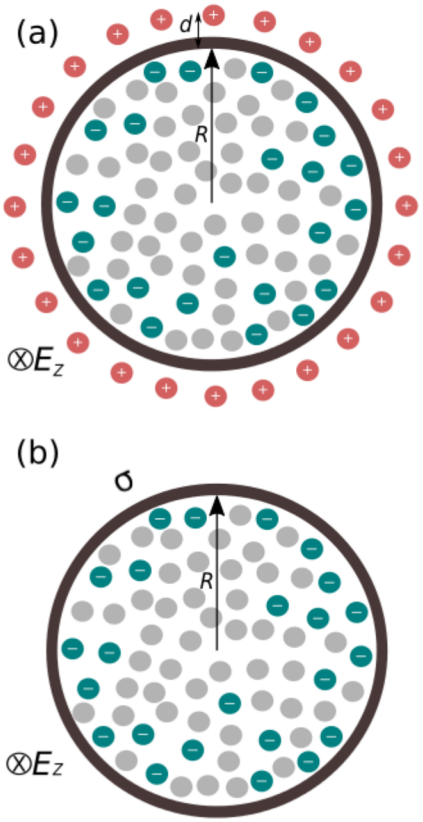

Fig. 1. Schematic illustration of the simulated system. Solvent particles and ions are confined in an infinite charged pore of radius R, oriented along the z axis. The electric field E_z is applied along the z direction, inducing an electroosmotic flow $u(r)$. (a) The cylinder surface charge is modeled with uniformly distributed point charges, located at distance d from the cylinder surface. (b) The cylinder charge is modeled as a continuous uniform surface charge density σ.

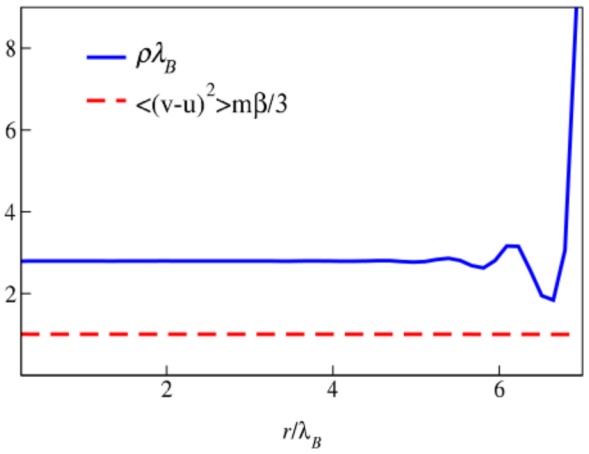

Fig. 2. Fluid concentration and temperature profiles along the r direction, represented by solid blue and dashed red curves, respectively. The temperature is related to the fluctuation of v with respect to the mean fluid velocity $u(r)$. Note that the temperature is uniform inside the pore. For all systems with the same concentration ρ_s the curves are very similar.

where $\mathbf{k} = (\frac{2\pi}{L_p}n_x, \frac{2\pi}{L_p}n_y, \frac{2\pi}{L_z}n_z)$ are the reciprocal vectors and ns are positive and negative integers, including zero. $V = L_p^2L_z$ is the volume and $\kappa_e = 5/L_z$ is the Ewald summation damping parameter. This is the classic Ewald summation method.

The term $\mathbf{k} = (0, 0, 0)$ in the sum require special care. This term diverges and the limit must be taken properly to account for the

macroscopic shape of the system i.e. if the replicated system has a form of a 3d rectangular prism, a slab, or a cylinder. Following the work of Smith on ionic crystals [4], two of the present authors introduced a method [33] to obtain the electrostatic potential of an infinitely replicated system of a specific macroscopic shape to be used in simulations:

$$\phi(\mathbf{r}) = \sum_{\mathbf{k}\neq 0}^{\infty}\sum_{j=1}^{N}\frac{4\pi q_j}{\epsilon V|\mathbf{k}|^2}exp\left[-\frac{|\mathbf{k}|^2}{4\kappa_e^2}+i\mathbf{k}\cdot(\mathbf{r}-\mathbf{r}_j)\right] - \sum_{j=1}^{N}\frac{2q_j}{\epsilon V\pi^2}\left[B_x(x-x_j)^2+B_y(y-y_j)^2+B_z(z-z_j)^2\right] + \sum_{j=1}^{N}q_j\frac{erfc(\kappa_e|\mathbf{r}-\mathbf{r}_j|)}{\epsilon|\mathbf{r}-\mathbf{r}_j|} \quad (2)$$

The shape dependent constants B's are given by

$$B_n = \int_{-\infty}^{+\infty} d^3\mathbf{k}\frac{k_n^2}{|\mathbf{k}|^2}\prod_{i=1}^{3}\frac{\sin(k_i\alpha_i L_c/2)}{k_i}, \quad (3)$$

where $\alpha_i L_c$ represent the lengths of the macroscopic 3d rectangular prism. The factors α_i/α_j represent the aspect ratios of the macroscopic system. In Ref. [33] the authors derived the corresponding expressions for the slab geometry, i.e. when $\alpha_z$remains finite, while $\alpha_x \to \infty, \alpha_x \to \infty$, and $\alpha_x/\alpha_y = 1$. In the present work, we are interested in a pseudo 1d periodic geometry. In this case α_x and α_y remain finite, with $\alpha_x/\alpha_y = 1$, while $\alpha_z \to \infty$. In order to take the limit, we rewrite the Eq. (3) using the identity,

$$\frac{1}{|\mathbf{k}|^2} = \int_0^{\infty} dt\, \exp(-t\mathbf{k}^2). \quad (4)$$

The B coefficients then become,

$$B_x = \frac{\pi^{5/2}\alpha_x L_c}{4}\int_0^{\infty}\frac{dt}{t^{3/2}}\exp(\frac{-\alpha_x^2 L_c^2}{16t})\mathrm{erf}(\frac{\alpha_y L_c}{4\sqrt{t}})\mathrm{erf}(\frac{\alpha_z L_c}{4\sqrt{t}}), \quad (5)$$

$$B_y = \frac{\pi^{5/2}\alpha_y L_c}{4}\int_0^{\infty}\frac{dt}{t^{3/2}}\exp(\frac{-\alpha_y^2 L_c^2}{16t})\mathrm{erf}(\frac{\alpha_x L_c}{4\sqrt{t}})\mathrm{erf}(\frac{\alpha_z L_c}{4\sqrt{t}}), \quad (6)$$

$$B_z = \frac{\pi^{5/2}\alpha_z L_c}{4}\int_0^{\infty}\frac{dt}{t^{3/2}}\exp(\frac{-\alpha_z^2 L_c^2}{16t})\mathrm{erf}(\frac{\alpha_x L_c}{4\sqrt{t}})\mathrm{erf}(\frac{\alpha_y L_c}{4\sqrt{t}}). \quad (7)$$

Setting $t = t'(\frac{\alpha_x^2 L_c^2}{16})$ in Eq. (5), $t = t'(\frac{\alpha_y^2 L_c^2}{16})$ in Eq. (6) and $t = t'(\frac{\alpha_z^2 L_c^2}{16})$ in Eq. (7) we obtain

$$B_x = \pi^{5/2}\int_0^{\infty}\frac{dt'}{t'^{3/2}}\exp(-\frac{1}{t'})\mathrm{erf}(\frac{\alpha_{yx}}{\sqrt{t'}})\mathrm{erf}(\frac{\alpha_{zx}}{\sqrt{t'}}), \quad (8)$$

$$B_y = \pi^{5/2}\int_0^{\infty}\frac{dt'}{t'^{3/2}}\exp(-\frac{1}{t'})\mathrm{erf}(\frac{\alpha_{xy}}{\sqrt{t'}})\mathrm{erf}(\frac{\alpha_{zy}}{\sqrt{t'}}), \quad (9)$$

$$B_z = \pi^{5/2}\int_0^{\infty}\frac{dt'}{t'^{3/2}}\exp(-\frac{1}{t'})\mathrm{erf}(\frac{\alpha_{xz}}{\sqrt{t'}})\mathrm{erf}(\frac{\alpha_{yz}}{\sqrt{t'}}), \quad (10)$$

where $\alpha_{ij} = \alpha_i/\alpha_j$. For an infinitely long cylinder oriented along the z direction, the aspect ratios are $\alpha_{yx} = \alpha_{xy} = 1, \alpha_{zx} = \alpha_{zy} \to \infty$, $\alpha_{xz} = \alpha_{yz} \to 0$, resulting in $B_x = B_y = \pi^3/2$ and $B_z = 0$.

The electrostatic energy of a pseudo 1d periodic system then reduces to $U = \sum_{i=1}^{N} q_i\phi(\mathbf{r}_i)$,

$$U = \sum_{i=1}^{N}\sum_{j>i}^{N}\frac{q_i q_j}{\epsilon}\frac{erfc(\kappa_e r_{ij})}{r_{ij}} + \sum_{\mathbf{k}\neq\mathbf{0}}\frac{2\pi}{\epsilon V|\mathbf{k}|^2}exp(-\frac{|\mathbf{k}|^2}{4\kappa_e^2})[A(\mathbf{k})^2+B(\mathbf{k})^2] + \frac{\pi}{\epsilon V}(M_x^2+M_y^2-Q_tG_x-Q_tG_y)\ , \quad (11)$$

where

$$A(\mathbf{k}) = \sum_{i=1}^{N} q_i cos(\mathbf{k}\cdot\mathbf{r}_i),\ B(\mathbf{k}) = -\sum_{i=1}^{N} q_i sin(\mathbf{k}\cdot\mathbf{r}_i),$$
$$M_x = \sum_{i=1}^{N} q_i x_i,\ M_y = \sum_{i=1}^{N} q_i y_i, G_x = \sum_{i=1}^{N} q_i x_i^2,\ G_y = \sum_{i=1}^{N} q_i y_i^2 \quad (12)$$

while $Q_t = \sum_{i=1}^{N} q_i$ is the total charge inside the system. Note that this expression is valid for a general charge non-neutral pseudo 1d periodic system. The last two terms of Eq. (11), which depend on Q_t, account for the non-neutral (NN) correction to the usual Ewald summation [33]. In order to use the modified 3d Ewald method, we must also include a sufficiently large empty space in x and y directions, to prevent the interaction between the spurious replicas introduced by the 3d Ewald summation. For the study of charged nanopores, we confine the particles in the region $\sqrt{x^2+y^2} < R$, with the vacuum extending between $R < \sqrt{x^2+y^2} < L_p$, where we set $L_p = 2L_z$. For larger L_p/L_z more $\mathbf{k}$-vectors are needed to achieve convergence, slowing down the simulations without any additional gain in accuracy.

4. Mean field theory

Consider an infinite cylinder of radius R, placed along the z axis, with surface charge density $\sigma > 0$. Confined inside the cylinder there are N_c counterions of charge $-e$, and $N_\pm$ ions of charges e and $-e$, where e is the proton charge. An electric field E_z is applied along the principal axis of the cylinder, inducing an electroosmotic flow $u(r)$ in z direction. The electrostatic potential in cylindrical coordinates is $\varphi(r,\theta,z) = \phi(r) - E_z z$, where $\phi(r)$ is the stationary electrostatic potential produced by all the charges inside the system. We will assume that the ions in the stationary state are distributed in accordance with the Boltzmann distribution. The self-consistent electrostatic potential then satisfies the Poisson-Boltzmann (PB) equation in cylindrical coordinates,

$$\epsilon\nabla^2\phi(r) = -4\pi\rho_q(r), \quad (13)$$

where ϵ is the water dielectric constant and ρ_q is the ionic charge density, $\rho_q(r) = e(A\exp[-\beta e\phi(r)] - B\exp[\beta e\phi(r)])$, where A and B are normalization factors. The equation can be solved numerically. On the other hand, the Stokes equation in the steady-state is given by

$$\eta\nabla^2 u(r) = -E_z\rho_q(r), \quad (14)$$

where $u(r)$ is the radial fluid velocity profile and η is the fluid dynamic viscosity. Combining Eq. (13) and Eq. (14), the fluid velocity can be expressed in terms of the electrostatic potential,

$$u(r) = \frac{\epsilon E_z}{4\pi\eta}[\phi(r) - \phi(R-d)]. \quad (15)$$

5. Results

We start by considering a system with only counterions. The nanopore has surface charge σ, and oppositely charged monovalent counterions in its interior. An electric field is applied in $z < 0$ direction, inducing a fluid electroosmotic flow. In the first approach the surface charge is modeled using point sites, each of charge e, uniformly distributed over the surface. The point sites are shifted slightly from the cylinder surface by a distance d, as can be seen in Fig. 1(a), in order to avoid the overlap with oppositely charged counterions. The DPD simulations are performed as described earlier and the electrostatic forces are calculated using the electrostatic energy derived in the Section 3, by

$\mathbf{F}_i = -(\partial U/\partial x_i, \partial U/\partial y_i, \partial U/\partial z_i)$, where $\mathbf{F}_i$ is the electrostatic force felt by particle i. In the present case, the non neutrality correction is not necessary since the total charge of the system — surface charge of point sites plus counterion charge — results in $Q_t = 0$. The dynamic viscosity η can be obtained with a Poiseuille flow simulation with no-slip boundary conditions, using the same DPD parameters [50]. There is also an alternative approach which gives the same result [51].

The stationary ionic density profile is represented by the orange squares in Fig. 3(a) while the fluid velocity in the z direction, at distance r from the center of the pore, is represented with the same symbols in Fig. 3(b). Together with the previous data we plot the concentrations and velocity profiles obtained using the mean-field theory, Eq. (13) and Eq. (14), represented by the black solid curve in Fig. 3(b) and Fig. 3(b). The reason why the surface point charges model is widely used to represent charged surfaces, in general, is related to the fact that the entire system is charge neutral. In this scenario, the classical Ewald summation method can be used to handle electrostatic forces [1,52–54]. However, for symmetries other than cubic, the expressions still must be corrected. The correction for cylindrical geometry is represented by the last line of Eq. (11) with $Q_t = 0$. Finally, it is interesting to observe that the Manning parameter for the present system is around 8.4, but the mean-field PB equation remains quite accurate. Accuracy of the mean-field theory was also observed for charged cylinder, used to model rigid polyelectrolyte with external counterions [55]. It reflects a general validity of PB equations for small monovalent ions [56].

We now introduce an alternative approach. Instead of using explicit point charges on the surface of the nanopore, a uniform homogeneous surface charge is introduced. From the Gauss law, such surface charge does not produce any electric field in the interior of the cylinder and its effect on the dynamics of ions inside the nanopore must be null. On the other hand, if the surface charge is ignored, the rest of the system is no longer charge neutral and one must take this explicitly into account in the Ewald summation. In our case, this is accomplished using the Q_t terms in Eq. (11), with $Q_t = -eN_c$. The blue circles in Fig. 3(a) represent the counterion density profile and in Fig. 3(b) the velocity profile. We see that the blue circles, representing the implicit surface charge approach, completely overlap with the orange squares, representing the explicit surface charges. On the other hand, if Q_t terms in Eq. (11) are neglected, a significant deviation between explicit and implicit charge approaches is observed, see green triangles in Fig. 3(b) and Fig. 3(b).

The bottleneck of simulations of systems with long-range interactions is the calculation of Ewald summation. By removing the necessity of explicitly accounting for the surface charges, we have dramatically reduced the number of interactions between the particles of the system that must be taken into account. In the present case, this leads to a gain in CPU time of approximately 40%, which is expected to increase even more if additional salt ions are present in simulations.

The effect of salt can be seen in Fig. 4 and Fig. 5. The mean-field theory remains very accurate even in the presence of salt ions. Again, one sees the importance of NN correction when modeling surface charge implicitly. In Fig. 5 we compare the electroosmotic flow for the system with and without salt. The added salt screens the electrostatic interactions, diminishing the electroosmotic flow.

Finally, we explore the effect of the valence of the surface charge groups on the electroosmotic flow. To do this we perform simulation of systems with the *same average* surface charge density σ, but composed of point ions of different valence. Clearly, we expect that discreteness effects will be amplified with the increased valence of the surface sites. The reason for this is two fold — for a fixed σ the average separation between the surface sites must increase with increasing valence, leading to stronger discreteness effect. Furthermore, larger point charge of the surface sites will result in stronger correlations between mobile ions and the surface sites [56]. Surprisingly, Fig. 6 shows that the valence of surface sites is negligible up to $+4e$. For this high valence more counterions become adsorbed to strongly charged surface sites, reducing the electroosmotic flow, see Fig. 6(b). We conclude that the implicit charge DPD simulation method developed in the present work should work well even for realistic surfaces with discrete multivalent ionic surface groups.

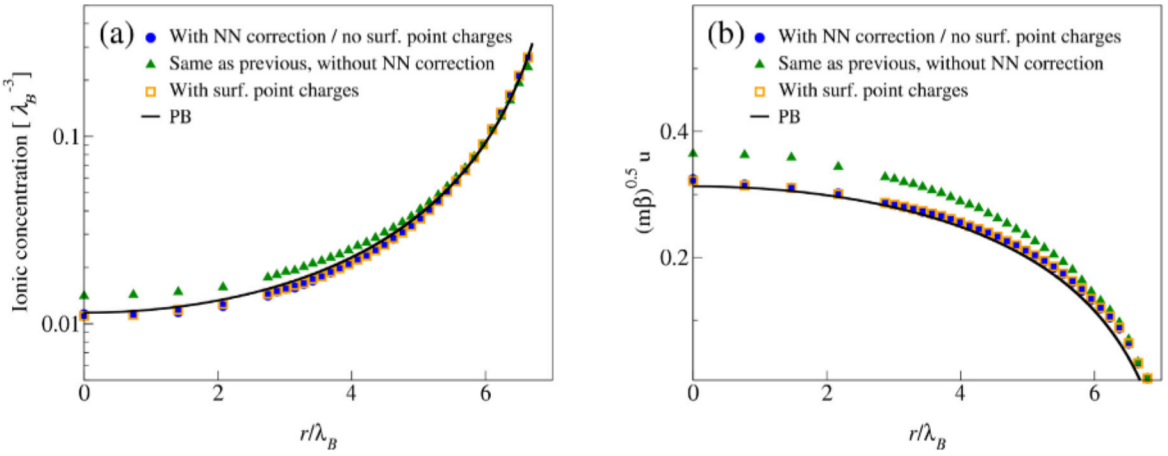

Fig. 3. (a) Counterion concentration profile along the r direction. Orange squares correspond to the first approach in which the surface charge is modeled using point surface sites. The blue circles correspond to the second approach in which the surface charge is treated implicitly. From Gauss' law, such charge distribution does not produce any electric field inside the pore. On the other hand, the rest of the system is no longer charge neutral and Ewald summation must account for this non-neutrality. This is done using Q_t terms in Eq. (11). Green triangles show the deviation that is observed if non-neutral terms are neglected in Eq. (11). Finally, the solid black line is the prediction of the mean-field theory. For monovalent ions, correlations are negligible and we observe very good agreement between the theory and simulations. The surface charge density is 0.0594 C/m^2 while the pore radius is $R/\lambda_B = 7$. (b) Velocity profile along r direction. Note that the blue and orange symbols are indistinguishable – explicit surface and implicit surface lead to the same electroosmotic flow as long as NN corrections are properly taken into account in the Ewald summation.

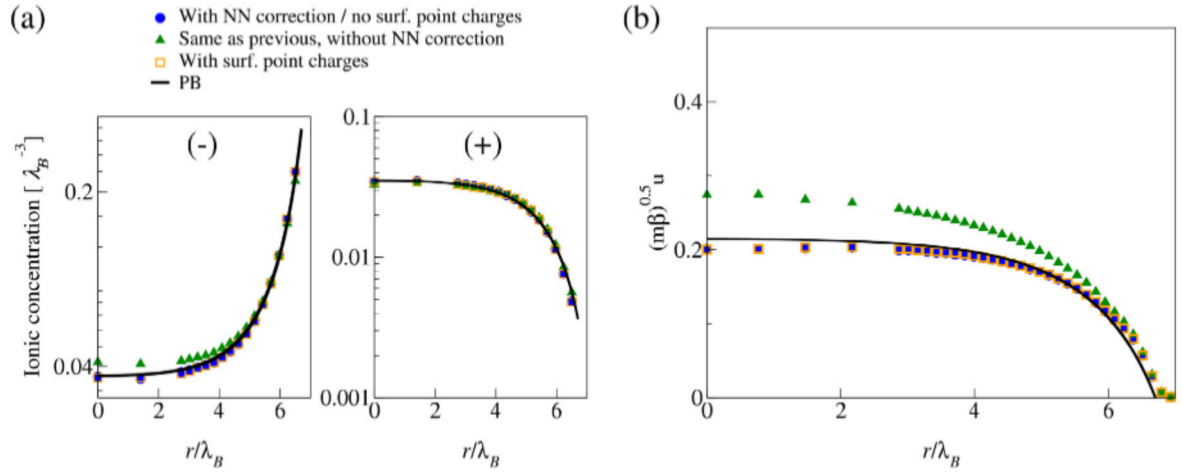

Fig. 4. (a) Ionic density profile along the r direction for a system with salt. Blue circles, green triangles, and orange squares represent the cases with: implicit surface charge and NN correction; implicit surface charge and *neglecting* NN correction; and simulation using explicit surface point charges, respectively. The solid black line is the prediction of the mean-field theory. The surface charge density is 0.0594 C/m^2, while the pore radius is $R/\lambda_B = 7$. The salt concentration is $0.02\lambda_B^{-3}$, approximately 89 mM. (b) Axial fluid velocity for different r. Note that the blue (implicit charge with NN) and orange (explicit charge) symbols are indistinguishable.

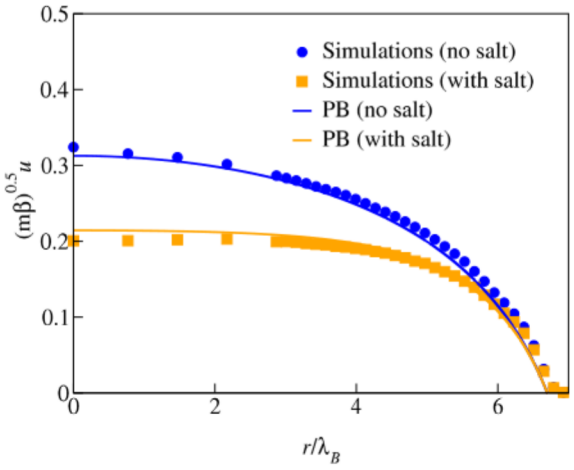

Fig. 5. Fluid velocity profiles without salt (blue circles) and with salt (orange squares). The parameters are the same as in Figs. 3 and 4.

6. Conclusions

We have developed a Dissipative Particle Dynamics simulation method to study electroosmotic flow inside cylindrical nanopores with surface charge. To properly treat the long-range electrostatic interactions between all the charges, we explored two different approaches. In the first approach the uniform surface charge was represented using surface point sites. The Coulomb interaction was then treated using 3d Ewald summation with an appropriate correction to account for the pseudo 1d geometry. In the second approach, the uniform surface charge was treated implicitly. For an infinitely long cylindrical nanopore, uniform surface charge leads to a vanishing electric filed in the pore's interior and can, therefore, be ignored in the DPD simulations. However, since the rest of the system in this case is no longer charge-neutral, a particular care must be taken in order to account for this non-neutrality while performing Ewald summation to calculate the electrostatic energy. We have shown how this can be handled efficiently within the formalism presented in the paper. It is found that the use of implicit surface charge leads to approximately 40% gain in effi-

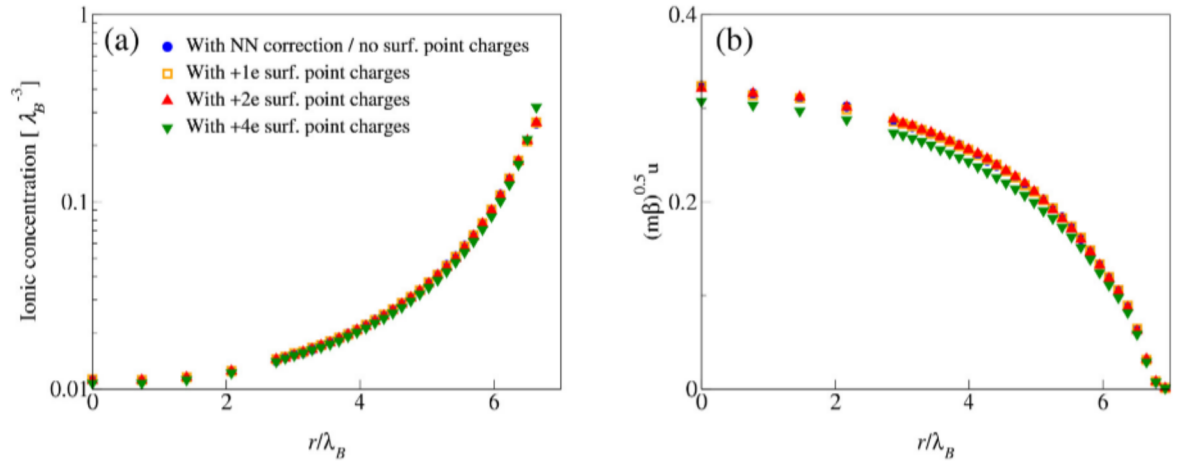

Fig. 6. (a) Ionic density profiles and (b) velocity profiles for the same parameters as in Fig. 3. The results for nanopores with the same average surface charge are compared: blue circles – uniform continuous surface charge density; orange squares – point charges of valence 1; red triangles – point charges of valence 2; green inverted triangles – point charges of valence 4. For 4-valent surface point charges we observe a small deviation from continuous charge distribution. The blue, orange, and red symbols are practically indistinguishable.

ciency of DPD simulations. A mean-field theory which agrees very well with the results of DPD simulations was also presented. In the future work, the dielectric polarization effects on the electroosmotic flow in charged nanopores will be explored.

CRediT authorship contribution statement

Igor M. Telles: Software, Validation, Investigation, Writing - original draft. **Rogério K. Bombardelli:** Software, Validation, Investigation, Writing - original draft. **Alexandre P. dos Santos:** Software, Conceptualization, Methodology, Resources, Writing - original draft, Supervision, Project administration, Funding acquisition. **Yan Levin:** Conceptualization, Writing - review & editing, Supervision, Funding acquisition.

Declaration of Competing Interest

The authors declare that they have no known competing financial interests or personal relationships that could have appeared to influence the work reported in this paper.

Acknowledgments

This work was supported by Brazilian Research Council (CNPq) under the grant 302720/2018-9, National Institute of Science and Technology Complex Fluids INCT-FCx, and by FAPERGS.

References

[1] P.P. Ewald, Ann. Phys. 369 (1921) 253.
[2] T. Darden, D. York, L. Pedersen, J. Chem. Phys. 98 (1993) 10089.
[3] U. Essmann, L. Perera, M.L. Berkowitz, T. Darden, H. Lee, L.G. Pedersen, J. Chem. Phys. 103 (1995) 8577.
[4] E.R. Smith, P.R. Soc. Lond. 375 (1981) 475.
[5] J. Kolafa, J.W. Perram, Mol. Simulat. 9 (1992) 351.
[6] T.E. Cheatham, J.L. Miller, T. Fox, T.A. Darden, P.A. Kollman, J. Am. Chem. Soc. 117 (1995) 4193.
[7] Y.T. Abdulnour, A.B. John, Comput. Phys. Commun. 95 (1996) 73.
[8] E. Spohr, J. Chem. Phys. 107 (1997) 6342.
[9] D. Frenkel, B. Smit, Understanding Molecular Simulation: From Algorithms to Applications, Academic Press. Inc., 2001.
[10] A. Bródka, Chem. Phys. Lett. 363 (2002) 604.
[11] R.M. Malossi, M. Girotto, A.P. dos Santos, Y. Levin, J. Chem. Phys. 153 (2020) 044121.
[12] L. Greengard, V. Rokhlin, J. Comput. Phys. 73 (1987) 325.
[13] A.W. Appel, J. Sci. Comput. 6 (1985) 85.
[14] L. Greengard, Science 265 (1994) 909.
[15] D. York, W. Yang, J. Chem. Phys. 101 (1994) 3298.
[16] C.I. Draghicescu, M. Draghicescu, J. Comput. Phys. 116 (1995) 69.
[17] Z.-H. Duan, R. Krasny, J. Chem. Phys. 113 (2000) 3492.
[18] B.A. Wells, A.L. Chaffee, J. Chem. Theory Comput. 11 (2015) 3684.
[19] M. González-Melchor, E. Mayoral, M.E. Velázquez, J. Alejandre, J. Chem. Phys. 125 (2006) 224107.
[20] E. Torres, I. Carrillo-Berdugo, D. Zorrilla, J. Sánchez-Márquez, J. Navas, J. Mol. Liq. 114643 (2020).
[21] T. Yamaguchi, H. Yamada, T. Fujiwara, K. Hori, J. Mol. Liq. 312 (2020) 113288.
[22] A. El-hoshoudy, E. Mansour, S. Desouky, J. Mol. Liq. 308 (2020) 113082.
[23] V. Dahirel, O. Bernard, M. Jardat, J. Mol. Liq. 303 (2020) 111942.
[24] P.H. Hünenberger, J.A. McCammon, J. Chem. Phys. 110 (1999) 1856.
[25] J. Picálek, J. Kolafa, J. Mol. Liq. 134 (2007) 29.
[26] B.W. McCann, O. Acevedo, J. Chem. Theory Comput. 9 (2013) 944.
[27] M. Girotto, T. Colla, A.P. dos Santos, Y. Levin, J. Phys Chem. B121 (2017) 6408.
[28] M. Girotto, A.M. Alencar, J. Phys. Chem. B 124 (2020) 7842.
[29] A.A. Freitas, K. Shimizu, J.N. Canongia Lopes, J. Mol. Liq. 301 (2020) 112402.
[30] X. Zeng, X. Zheng, L. Guo, Q. Xu, H. Huang, B. Tan, J. Mol. Liq. (2020) 115063.
[31] I.-C. Yeh, M.L. Berkowitz, J. Chem. Phys. 111 (1999) 3155.
[32] A. Bródka, Chem. Phys. Lett. 400 (2004) 62.
[33] A.P. dos Santos, M. Girotto, Y. Levin, J. Chem. Phys. 144 (2016) 144103.
[34] M. Kawata, M. Mikami, Chem. Phys. Lett. 340 (2001) 157.
[35] A. Arnold, J. de Joannis, C. Holm, J. Chem. Phys. 117 (2002) 2496.
[36] A.P. dos Santos, Y. Levin, J. Chem. Phys. 144 (2015) 194104.
[37] M. Porto, J. Phys. A-Math. Gen. 33 (2000) 6211.
[38] M.C. Gordillo, J. Martí, Chem. Phys. Lett. 329 (2000) 341.
[39] J. Wang, A.G. Kalinichev, R. Kirkpatrick, Geochim. Cosmochim. Ac68 (2004) 3351.
[40] A. Arnold, C. Holm, J. Chem. Phys. 123 (2005) 144103.
[41] A. Bródka, J. Chem. Phys. 125 (2006) 107103.
[42] J. Wong-ekkabut, M. Karttunen, J. Chem. Theory Comput. 8 (2012) 2905.
[43] V. Ballenegger, A. Arnold, J.J. Cerdà, J. Chem. Phys. 131 (2009) 094107.
[44] J.S. Hub, B.L. de Groot, H. Grubmüller, G. Groenhof, J. Chem. Theory Comput. 10 (2014) 381.
[45] S. Yi, C. Pan, Z. Hu, J. Chem. Phys. 147 (2017) 126101.
[46] R.D. Groot, P.B. Warren, J. Chem. Phys. 107 (1995) 4423.
[47] P. Español, P. Warren, Europhys. Lett. 30 (1995) 191.
[48] P. Español, Phys. Rev. E 52 (1995) 1734.
[49] I. Pivkin, G. Karniadakis, J. Comput. Phys. 207 (2005) 114.
[50] J. Smiatek, M.P. Allen, F. Schmid, Eur. Phys. J. E: Soft Matter 26 (2008) 115.
[51] J.A. Backer, C.P. Lowe, H.C.J. Hoefsloot, P.D. Ledema, J. Chem. Phys. 122 (2005) 154503.
[52] J. Ennari, I. Neelov, F. Sundholm, Polymer 41 (2000) 4057.
[53] M. Kawata, U. Nagashima, Chem. Phys. Lett. 340 (2001) 165.
[54] Y. Yao, J. Capecelatro, Phys. Rev. Fluids 3 (2018) 034301.
[55] M. Deserno, C. Holm, S. May, Macromolecules 33 (2000) 199.
[56] Y. Levin, Rep. Prog. Phys. 65 (2002) 1577.